Simulation of Single Gimbal Control Moment Gyroscopes (SGCMG) Cluster for Microsatellite Maritime Surveillance Mission

Ki Hwan Keum, Regina Lee
York University
4700 Keele Street, Toronto, ON, Canada; +12892212062
pkeum@yorku.ca

ABSTRACT

The potential for agile missions for small satellites exists through development of single gimbal control moment gyroscopes (SGCMG). An SGCMG cluster comes with additional complexity and volume requirements, but efforts in their development have reduced their overall size while providing higher torque over similarly sized reaction wheels. In this paper, we present a feasibility study of a small satellite using a small volume pyramid SGCMG cluster for coastline monitoring through Simulink. Two realistic torque profiles for sweeping capture of complex coastlines within one minute were generated using STK, requiring maximum torques of 0.190 and 0.218 Nm and rapid slew rate. The torques are beyond the capabilities of a similarly sized reaction wheel, which can only output maximum torques of 0.020 Nm. The torque profiles were replicated using simulated SGCMG cluster using modelled SGCMG scaled for small satellites. Results show that the SGCMG pyramid cluster meets the required torque profiles with less than 0.3 degrees of pointing error throughout the maneuver. A novel SGCMG hardware is currently under development and preliminary analysis indicates sufficient torque for agile missions such as coastal monitoring presented in this paper. The viability of SGCMG cluster provide promising alternative for ACS design of small satellites where agility have been limited by existing attitude actuators.

INTRODUCTION

Current trends in space missions lean towards heavy usage of small satellites.[1] While specific mass classification varies, satellites under 500 kg are typically considered a small satellite.[2] Remote sensing, broadband communications, and Earth observations are just some examples of small satellite applications.[1,2] Main advantage of small satellites over conventional large satellites is the reduction in both time and material costs in development.[2]

There are two main types of actuators on small satellites: magnetorquers and reaction wheels.[3] While thrusters are also used as actuators for satellites, they also add a layer of complexity due to changing mass as well as their effect on satellite orbit. Given current small satellite uses, thrusters are rare for small satellites. While small satellites typically use a combination of magnetorquers and reaction wheels to meet their attitude determination and control system (ADCS) requirements, limitations exist in terms of maximal torque generation and power consumption, restricting possible mission profiles.

A potential actuator to address this limitation in small satellite attitude control is the control moment gyroscope (CMG), which are similar to reaction wheels but instead of changing the angular velocity of the flywheel, the orientation of the flywheel is changed through gimbals. Previous work exists which provides proof of demonstration of a working CMG actuator in a small satellite platform.[4,5] However, while the actuator itself has achieved the stage of commercial use in some of larger satellites, usage in satellites under 100 kg remains mostly theoretical.

Simulation results and some real-life results on Earth are available for small satellite of single gimbal control moment gyroscopes (SGCMG) clusters. V. Lappas et al. developed a small 4-SGCMG cluster which weighed about 1 kg including all components. Simulated results of the cluster output about 0.09 Nm torque in a single-axis movement for a maximum angular rate of 10.11 deg/s.[6] University of Florida developed a high-fidelity simulation of their 1U CubeSat, SwampSat, which uses a SGCMG cluster for actuation.[7] The full ADCS loop was simulated, from orbit simulation to attitude control. A 90-degree rest-to-rest maneuver was simulated, along with a practical sun-tracking maneuver with the SGCMG cluster. It was shown that the 90-degree slew was able to be achieved in 20 seconds with less than 1-degree error in attitude. In the sun-tracking mode, the sun was able to be tracked with just slightly greater than 1-degree error.

A component missing in previous SGCMG analysis is a practical use case for small satellites. This paper expands upon the CMG analysis through simulation of a single gimbal CMG (SGCMG) cluster designed for small satellites. A feasibility analysis is performed through

simulation of its torque output in a coastline observation use case. The goal was to quantify the benefits of CMG over existing reaction wheels through the demonstration of a practical use case where the small-scale CMG cluster meets torque requirements that similarly sized reaction wheels cannot. This can help justify further CMG development for small satellites.

It is expected that SGCMG cluster simulated in this thesis will produce better pointing accuracy as attitude determination as assumptions for both hardware and attitude control is made to simplify the analysis.

SGCMG PYRAMID CLUSTER MODEL

Dynamics of satellite and SGCMG

SGCMG is the type of CMG most commonly being researched for usage in smaller satellites This is due to its mechanical simplicity compared to other types of CMGs, reducing its failure points.[8] Figure 1 shows a concept image of a SGCMG along with arrows indicating the directions of the gimbal axis, the angular momentum of the flywheel, h, and the torque output of the SGCMG, T. The $\dot{\delta}$ term represents the gimbal velocity about the axis. As the gimbal velocity varies, the direction of h changes with time, which leads to change in direction of the torque output with time as well.
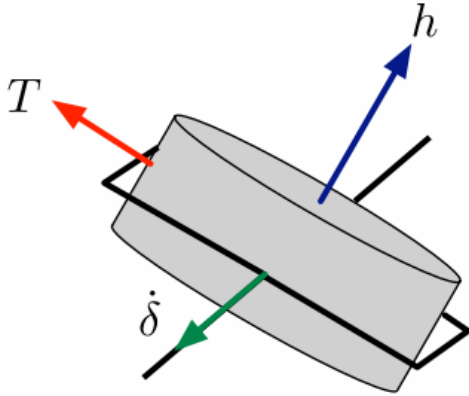

Figure 1: Overview of vectors involved in SGCMG operation[9]

The principal equation describing the satellite's rigid body motion involving a momentum-exchange actuator is given as:

$$J\dot{\omega} = \tau - \omega \times (J\omega + h_{act}) - \dot{h}_{act} \qquad (1)$$

where J is the inertia matrix of the satellite, ω is the angular velocity, $\dot{\omega}$ is the angular acceleration, τ is any external torque applied on the spacecraft, h_{act} represents actuator momentum, and $\dot{h}_{act}$ represents actuator torque,

all in the body frame. This equation can be rewritten as the following:

$$J\dot{\omega} = (\tau + T_{act}) - \omega \times J\omega \qquad (2)$$

where the torque vector is found as shown:

$$T_{act} = -\omega \times h_{act} - \dot{h}_{act} \qquad (3)$$

The h_{act} term becomes the angular momentum of the flywheel, and the $\dot{h}_{act}$ term becomes the torque output through gimbal motion of the CMG, expanded as follows:

$$\tau_{CMG} = \dot{h}_{cmg} = h_{wheel} \times \dot{\delta}_{gimbal} \qquad (4)$$

This is the dominant term for torque output of the SGCMG; other terms are deemed negligible by ignoring all acceleration terms, as well as assuming that the mass of the SGCMG cluster is significantly smaller than the mass of the satellite. This is a common assumption that is made in context of a feasibility analysis, where torque output of the cluster is the parameter of focus. This assumption should be evaluated with hardware testing, which is outside the scope of the analysis.

SGCMG Modelling

The simulated SGCMG was sized accordingly to fit a small satellite. Table 1 displays the parameters associated with the single SGCMG. A saturation block was used to limit the voltage input into the plant model, and another separate saturation block was used to represent the physical limitation on gimbal speed. The flywheel was assumed to be in ideal operation, where it is at a constant rate throughout the analysis. The flywheel was also assumed to have fixed inertia along all principal axes. All the parameter values were based on a SGCMG that is currently in-development for small satellites by an industry partner. The proposed SGCMG design features compact dimension (less than 1U-CubeSat structure) of 1-kg mass with an estimated maximum torque of 0.220 Nm.

Table 1: Key parameters of the simulated SGCMG

Parameter	Value
Flywheel nominal angular rate [rad/s]	1000
Gimbal speed limit [rad/s]	2.19
Wheel diameter [m]	0.04699
Torque output [Nm]	0.220
Torque Constant [Nm/V]	0.0974

Inductance Constant [H]	0.35×10^{-3}
Armature Resistance [Ohms]	1.99
Flywheel Inertia [kgm^2]	9.12×10^{-5}
Gimbal motor inertia [kgm^2]	174.99×10^{-6}

Table 2 shows similarly sized reaction wheels in the market for comparison. While the SGCMG will still take up slightly more volume due to gimbals, it will have a higher output. Matching the torque output using the reaction wheels requires at least triple the diameter of the wheel, which would result in a much larger volume than the SGCMG.

Table 2: Comparable reaction wheels in the market[10]

Wheel Model	Wheel Diameter [m]	Torque Output [Nm]
Blue Canyon Tech RWP015	0.042	0.0040
Blue Canyon Tech RW4	0.170	0.3000
MSCI MicroWheel 200	0.090	0.0300
MSCI MicroWheel 4000	0.218	0.1500
Sinclair Interplanetary (now Rocket Labs) RW-0.03	0.050	0.0020
Sinclair Interplanetary (now Rocket Labs) RW3-1.0	0.150	0.0500

Pyramid Cluster Torque Modelling

Many different SGCMG cluster configurations are available to control the satellite.[11,12] A commonly used configuration is the pyramid SGCMG setup, visualized in Figure 2. In the figure, following terms are shown: the $\vec{g}_i$ terms are the gimbal axis of each SGCMG in the cluster, the $\vec{h}_i$ terms are the instantaneous angular momentum of the flywheels, the x_i terms are the instantaneous gimbal angles, and the beta angle β is the skew angle from the principal axis of the CMG cluster. The skew angle allows each CMG to affect multiple axes at once instead of being limited to control of only one axis. A pyramid setup involves four SGMCGs, and it ensures the most evenly distributed momentum envelope as it provides complete coverage of the possible attitude profile.[13]
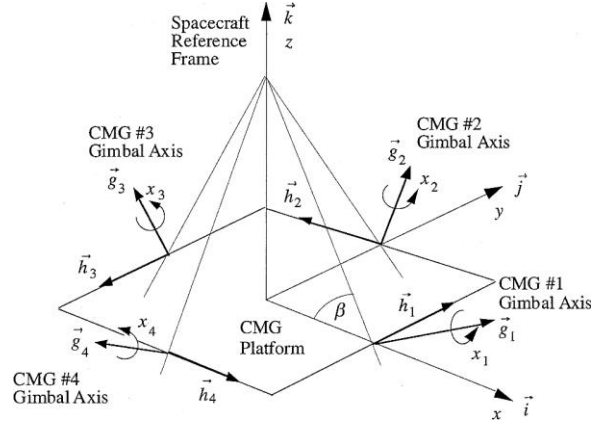

Figure 2: A four-SGCMG configured in a pyramid arrangement[11]

The total torque generated by the four SGCMG in the pyramid configuration is described is described as follows:

$$T = \frac{d\mathbf{H}}{dt} = \mathbf{A} \cdot \dot{\delta} \qquad (7)$$

Where T is torque, $\dot{\delta}$ is the rate of change of the gimbal, and The A matrix in equation (8) is the Jacobian matrix of the cluster as follows:

$$\mathbf{A} = \begin{bmatrix} -\cos\beta \cdot \cos x_1 & \sin x_2 & \cos\beta \cdot \cos x_3 & -\sin x_4 \\ -\sin x_1 & -\cos\beta \cdot \cos x_2 & \sin x_3 & \cos\beta \cdot \cos x_4 \\ \sin\beta \cdot \cos x_1 & \sin\beta \cdot \cos x_2 & \sin\beta \cdot \cos x_3 & \sin\beta \cdot \cos x_4 \end{bmatrix} \quad (8)$$

It is assumed that the beta angle is constant between the four SGCMG used in the pyramid cluster. For the simulated pyramid configuration, beta angle was set to be 53.13 degrees. useful in describing the motion of the gimbals which in turn produces torque. The SGCMGs placed in the pyramid cluster are not aligned with the body axis of the satellite, which means conversion between the two reference frames is necessary.

SIMULATION SETUP

STK Coastline Monitoring Scenario Setup

Coastal monitoring is a common type of mission capable of serving multiple interests, including coastal surveillance, prevention of maritime crisis and crime, and supporting aquaculture. Augmentation of coastal monitoring through satellites can be an effective way to track the rapidly changing coast in the days of climate change. Small satellites can help in this area, but the number of coastlines to monitor as well as their shape can be beyond the tracking capabilities of a reaction wheel. An SGCMG cluster can be an effective way to monitor complex coastlines in a short period through increase in potential number of points that can be pointed towards in a set interval.

AGI's STK software was used to develop the coastline monitoring mission. The satellite was placed in a sun-synchronous polar orbit to take spot-to-spot images of the targets of interest within its field of view of 1-degree cone half angle. The sensor size was arbitrarily chosen as it was not important for initial attitude analysis. The size of the spacecraft was based on STK's model of NEOSSat. This was done due to both the availability of the satellite configuration in STK as well as for the size of the spacecraft, as it is far greater than the CMG cluster. This means the inertia of the SGCMG cluster has negligible effects on overall satellite inertia matrix. Table 3 shows the highlighted parameters of the satellite used in simulation of the coastline monitoring.

Table 3: Satellite parameters used in STK and Simulink simulation

Parameter	Value
Camera sensor type	Simple conic, 1-degree cone half angle
Inertia per axis (X, Y, Z) [kgm^2]	(3.994, 4.810, 8.880)
Mass of Spacecraft [kg]	75

The simulation of the SGCMG pyramid cluster assumed nominal operation in the analysis period, where the flywheel speed is fixed at its operational speed and no noise is present in gimbal speed commands. It is also assumed that the size of the SGCMG cluster is significantly smaller than the overall satellite size. This would mean that any variations in the SGCMG inertia matrix as well as its momentum would not be significant in the satellite frame. Therefore, the satellite inertia matrix was assumed constant. While a high-fidelity modelling of the SGCMG cluster would provide a deeper analysis of its performance, for feasibility analysis this was deemed a good starting point.

Torque profiles from seven coastlines were generated, from which two were selected requiring the highest torques: Coastline E, consisting of the entire island of Prince Edward Island (PEI), and coastline F, consisting of the coastline of Newfoundland. A zoomed-up image of the two coastlines can be seen in Figure 3 and Figure 4, respectively. For Coastline E, the sweep began from the bottom-right point, going through each point in a clockwise manner. For Coastline F, the sweep began from the right-most point, meeting each target from right to left in a sequential manner. To test the limits of slew rate, a complete observation of the coastline was setup to occur in a very short period, under one minute. As a result, Coastline E (PEI) was traversed in 38 seconds, while coastline F (Newfoundland) was traversed in 36 seconds.

Figure 3: Zoomed-in screen capture of Coastline E from the STK scenario, representing PEI

Figure 4: Zoomed-in screen capture of Coastline F from the STK scenario, representing the partial coastline of Newfoundland and Labrador

It was assumed that the camera would be able to take images within a short timeframe, under one second, at each specified point in the coastline. The sweep of coastline E worked in clockwise manner, while the sweep of Coastline F worked in a right-to-left manner. The objective during the observation period was to have the satellite constantly adjust its pointing so that the sensor captures the whole coastline during the few seconds in each pass. The satellite was set in constant motion through the coastline, slowing down only briefly at each target point then accelerating away to the next specified point. Table 4 shows the highest and lowest torque needed to track the coastlines of Region E and Region F in this manner.

Table 4: Torque profile information of Coastline E and Coastline F

Region	Highest torque [Nm]	Average torque [Nm]	Highest slew rate [rad/s]	Average slew rate [rad/s]
E	0.190	0.0496	0.0402	0.0163
F	0.218	0.0827	0.0519	0.0226

MATLAB SGCMG Cluster Setup

Figure 5 shows the overall Simulink loop used to generate the SGCMG cluster output given the torque

profile generated by the STK scenario. The initial values of the quaternion and angular velocity of the satellite were set to match the initial satellite condition at the first timestep of the STK export file. The solver used in Simulink was the ODE45 solver, using variable step size with minimum step size of 0.001 seconds and a maximum step size of 1 second. The use of variable step size assisted in reducing the simulation runtime.
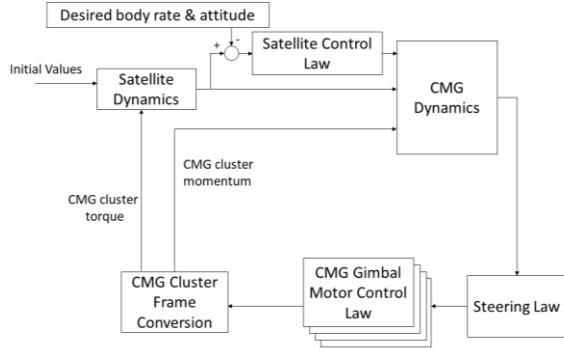

Figure 5: Algorithm loop visualization of the Simulink setup for the pyramid SGCMG cluster

Each CMG gimbal control block contains a control law block and a plant model. The control law used to control the gimbal is a simple proportional-integral-derivative (PID) control, which was sufficient for the response required from the gimbal for meeting the torque requirements. The plant model is based on a simple DC motor. The values of the constants in the model can be seen back in Table 1.

Table 5 shows the PID gains used for to control law block and the resulting response characteristics. The gain values were chosen for rapid response with minimal overshoot. Settling time was not a concern as each gimbal in the cluster CMG would need to respond to a wide range of requested speeds which would change rapidly throughout the analysis. Because the gimbal would follow a simple PID control, the built-in Simulink block for PID was used to fine-tune the gains.

Table 5: Gains used for PID control of the gimbal motor and resulting response characteristics

Gain/Characteristic	Value
Kp	500
Ki	30000
Kd	0.500
Rise time (s)	0.00445
% Overshoot	3.66

One of the components which increases the complexity of a SGCMG cluster over typical actuator is the requirement of a steering law. The purpose of the steering law is to find the speed required by each individual gimbal, or the $\dot{\delta}$ term from equation (7) for each gimbal in the cluster, while at the same time avoiding the occurrence of a singularity. Singularity is where the cluster loses capability of outputting torque over an axis at certain orientation of the gimbals in the cluster. Multiple steering laws have been developed and researched for SGCMG clusters.[13] The simplest steering law for the CMG cluster is the pseudoinverse steering law, which makes use of the Jacobian matrix from equation (8). The pseudoinverse steering law consists of the inversion of this matrix, which would solve for the necessary gimbal rates. Assuming a pyramid configuration, the gimbal rate command can be found using a pseudoinverse as shown:

$$\dot{\delta} = A^+ \mathbf{u} \tag{11a}$$

$$A^+ = A^T (AA^T)^{-1} \tag{11b}$$

Where A represents the Jacobian matrix from equation (8) and $\mathbf{u}$ represents the torque output required by the cluster. Whether the CMG cluster reaches singularity or not can be quickly checked by calculation for the determinant of AA^T. If this value reaches 0, then singularity is reached, which means the cluster's ability to output torque on one of the axes is lost.

It was found that the simple pseudoinverse steering law was insufficient for avoiding singularities when attempting to follow Coastline E and Coastline F. The occurrence of singularity results in large errors in pointing which cannot be remedied during the short duration of the coastline sweep. A more effective steering law was developed called the singularity robust inverse law, which builds from the pseudoinverse equation by adding on more terms.[14] The generalized singularity robust law results from adding on an additional term to the pseudoinverse, resulting in the following equations:

$$\dot{\delta} = A^\# \mathbf{u} \tag{12a}$$

$$A^\# = A^T [AA^T + \lambda E]^{-1} \tag{12b}$$

$$\lambda = \lambda_0 e^{-1000\lambda_0 |AA^T|} \tag{12c}$$

$$E = \begin{bmatrix} 1 & \epsilon_3 & \epsilon_2 \\ \epsilon_3 & 1 & \epsilon_1 \\ \epsilon_2 & \epsilon_1 & 1 \end{bmatrix} \tag{12d}$$

$$\epsilon_i = \epsilon_0 \sin(\omega t + \phi_i) \tag{12e}$$

Table 6 shows the selected values in the steering law. The values were chosen based off the methodology from the original paper.[14]

Table 6: Values used for the singularity robust steering law

Variable	Value
λ_0	0.01
ϵ_0	0.01
ω	$\frac{1}{2}\pi$
ϕ_1	0
ϕ_2	$\frac{1}{2}\pi$
ϕ_3	π

Initially, satellite control was to be bypassed by directly using the torque profile generated from the STK as the input. However, using the STK torque profile directly resulted in persisting errors due to its form as an open-loop control; there was no feedback to show that the torque profile was met, leading to culminating pointing error throughout the sweep. Therefore, it was necessary to create a closed-loop control using quaternion feedback. The dependency of STK remains as the desired angular velocity and the desired quaternions are taken straight from STK.

Using the rigid body dynamics, the body rates and quaternions can be used in the quaternion feedback law. Note that the attitude determination for this simulation was assumed ideal, in that the true value of the relevant states, the satellite angular velocity and the quaternion, is fully known. No sensors are involved to determine the satellite's parameters, and no determination algorithm is used. The focus is on the ability of the SGCMG cluster to output the necessary torques.

The governing equation of the quaternion feedback is shown in equation (13):

$$\mathbf{T} = -Kq_e - C\omega_e \tag{13}$$

where T is the required torque, K and C are gains, q_e is the quaternion which represents the rotation between the desired and actual quaternions found through quaternion multiplication, and ω_e is the difference between the desired and actual body rates. The desired angular velocity and the desired quaternion are pre-determined through the STK scenario. The gains K and C were set to be 3 and 300, respectively. This is because the satellite is in constant rotation, the angular velocity of the satellite was deemed to have a higher weight for torque over the orientation of the satellite. The constant motion to sweep through all the points in a brief period meant that the error in angular velocity would be the primary driver of the required torques. The gains were chosen as a ratio of impact between quaternion and angular velocity, and a short trial and error analysis showed the current ratio of

1:100 provided low errors while remaining stable. Values higher than 300 for C introduced heavy jitter on the spacecraft torque. The torque found through this control law is used in Equation (3) to determine the $\dot{\mathbf{h}}_{\mathbf{act}}$ term for use in the steering law.

COASTLINE MONITORING RESULTS

Figure 6 shows the commanded and actual gimbal speed of the four SGCMG in the cluster for Coastline E and Coastline F. In Coastline E, the SGCMG were able to follow the commanded speeds aside from a brief period near the 20 second mark for one of the gimbals. Coastline F showed more instances of saturated gimbal speeds. Between 25 to 30 seconds, heavy disruption to nominal operation is expected as multiple gimbals fail to meet the commanded velocities at various times in the interval.
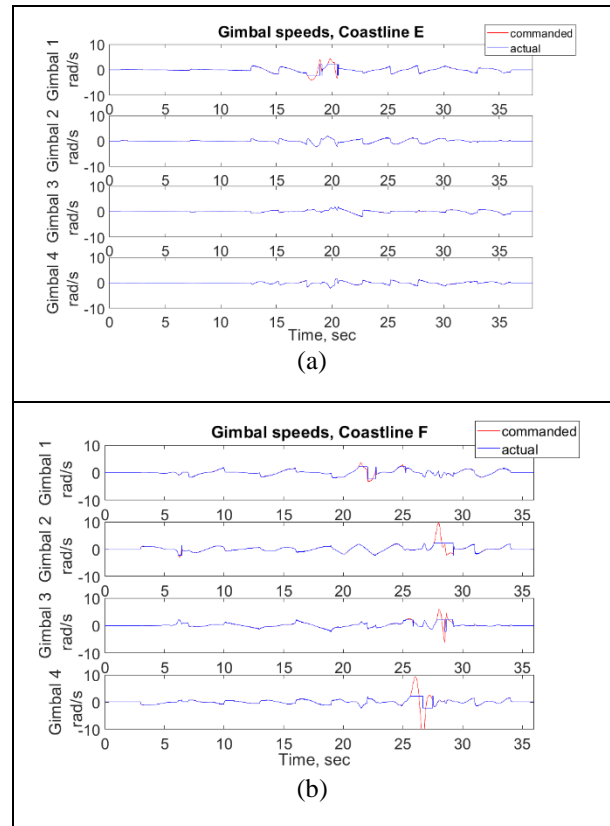

(a)

(b)

Figure 6: Desired vs actual gimbal speed of each gimbal in the pyramid cluster through: (a) sweep of Coastline E, and (b) sweep of Coastline F

Figure 7 shows the resulting torque profile throughout the sweep of Coastline E from the simulated SGCMG cluster as well as the ideal torque profile generated from the STK scenario for the same coastline, and Figure 8 shows the resulting torque generated by the SGCMG cluster throughout the sweep of Coastline F and the ideal torque profile generated from the STK scenario. The red

dotted line represents the maximum torque that can be generated by MSCI's MicroWheel 200 for comparison.
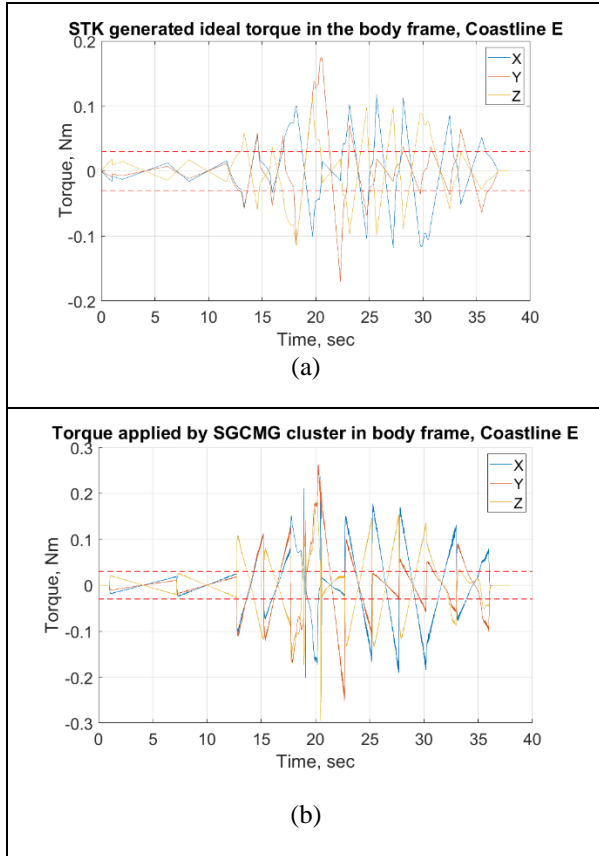

(a)

(b)

Figure 7: Pyramid SGCMG cluster's torque output in terms of body frame throughout sweep of Coastline E in: (a) STK scenario ideal torque profile (b) Simulink generated torque profile
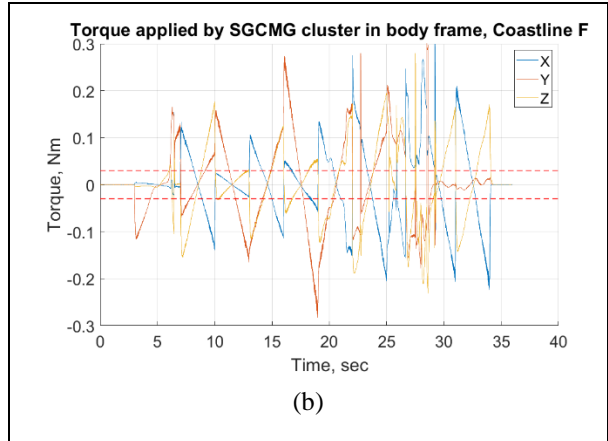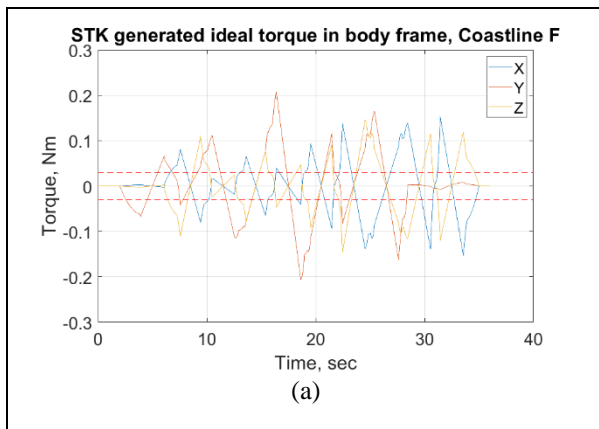

(a)

(b)

Figure 8: Pyramid SGCMG cluster's torque output in terms of body frame throughout sweep of Coastline F in: (a) STK scenario ideal torque profile (b) Simulink generated torque profile

Figure 9 shows the pointing error of the satellite throughout the sweep of the Coastline E and Coastline F. Rise in pointing error is seen when the SGCMG are unable to meet the requested speeds due to saturation.
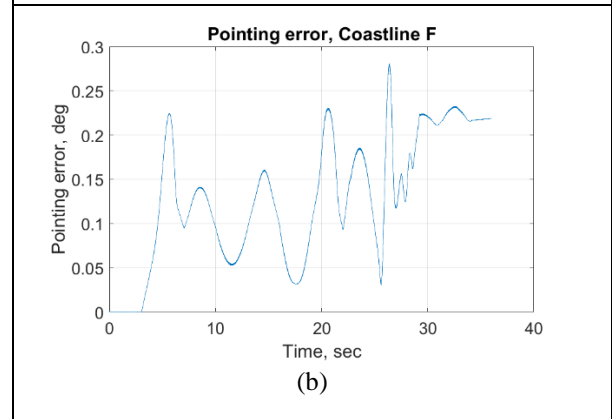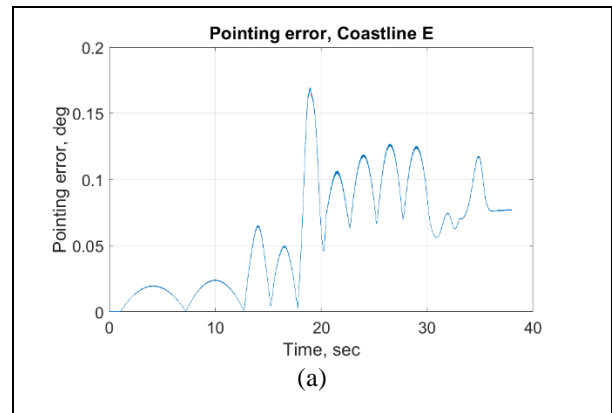

(a)

(b)

Figure 9: Pointing error throughout: (a) sweep of Coastline E, and (b) sweep of Coastline F

DISCUSSION

The torque profile was met by the cluster until individual SGCMGs were unable to meet the commanded speed due to limitation on gimbal rate. The quaternion feedback control law was able to compensate for the error after the brief period of command loss, allowing the pointing error to remain low for the rest of the sweep. One interesting point of note is that at the point where commanded gimbal speeds were not met, it was compensated through additional torque using the other gimbals available. This caused the maximum torque on an axis to surpass the expected maximum torque of the scenario during the maneuver shown in Table 4. This trend is shown for both coastlines.

As precise accuracy was not the main requirement throughout the sweep as the satellite is in constant motion. It was only necessary that the satellite briefly captures all the designated points in the coastline when sweeping through the region. Compared to Coastline E, Coastline F required significant change of slew rates to fully cover all the points. Combined with multiple occurrences of gimbal rate limits being reached resulted in an average increase in pointing error relative to Coastline E, especially in the period where multiple gimbal rate limits were met.

The simulated SGCMG cluster is shown to sweep both coastlines effectively. The maximum pointing error seen during the sweep of Coastline E is 0.17 degrees, while the maximum pointing error seen during the sweep of Coastline F is 0.28 degrees. This translates to about 2.33 km to 3.84 km of pointing error on the surface. The typical LEO high definition EO has a swath width of 13-16 km. This means that the satellite should be able to successfully capture the points with the given slew rates.

As expected, Coastline F which required higher average torques resulted in higher error compared to Coastline E. Interesting reactions occur for gimbal speeds at saturation, where it is unable to return to desired speeds for a short duration after it hits maximum speeds. This may be due to limitation on modelling of the SGCMG, as the saturation block only limits the output gimbal speed but not the theoretical gimbal speed. the theoretical gimbal speeds were shown to reach 300 rad/s to reduce the error between the commanded gimbal speed and the actual gimbal speed. As the PID control acted to correct this speed, overshoot is present, and from the perspective within 2 rad/s limits it becomes near-instant changes of velocity.

While not explicitly tested, reaction wheels are not able to achieve the torque profile of the coastlines. Using MSCI's MicroWheel 200 as reference, not only is the maximum torque output difficult, but the sharp shifts in torque when the satellite must accelerate or decelerate near a point is difficult to achieve with just reaction wheels. The results show that barring gimbal rate limits, an SGCMG cluster can meet the sharp torque requirements. Reaction wheels may also saturate, where they hit their maximum speeds, at which point must be desaturated before using them again. SGCMG cluster avoids this, giving them more uptime.

CONCLUSION

A feasibility study of using a 4-SGCMG cluster in pyramid configuration on a small satellite was shown through a coastline monitoring use case scenario. The simulated hardware was sized for small satellites to reduce its volume and could provide up to 0.220 Nm torque. The use case chosen for this analysis was coastal monitoring, and target torque profiles were generated using STK which tracked the Coastline of PEI and Newfoundland and Labrador. Combined with quaternion feedback control law and singularity robust inverse steering law, the pointing error was kept below 0.3 degrees throughout the sweep of both coastlines. The results showed that a small-scale SGCMG may also be worth developing given the results from the first look at a coastline sweep mission. While there are still multiple hurdles to overcome in terms of complexity of its operation and configuration, a small SGCMG cluster may extend the capabilities of small satellites for agile missions.

The additional agility of the SGCMG cluster can be taken advantage of in other use cases as well. One of these use case would be residential space object (RSO) tracking. Unlike Earth, RSO is in rapid transit relative to the position of the satellite, requiring quick movements to capture them. As well, RSO in LEO will require high agility to track due to reduced distance between the satellite and the object. An SGCMG hardware suitable for small satellites is currently in development by an industry partner, which includes physical model analysis as well as a separate high-fidelity simulation using more accurate plant models. The current simulation results will be a good step towards full development of the actuator.

A significant gap in SGCMG cluster analysis stems from lack of an attitude determination component. Addition of attitude determination such that the SGCMG control works from estimated states will provide more realistic view of its performance. Power consumption analysis can also solidify the benefits of SGCMG cluster for small satellites. This benefit is especially relevant for small satellites and can reinforce the justification of the use of a SGCMG cluster. Analysis can also be expanded through exploration of other highly agile scenarios for satellites, which can be developed through STK. As

mentioned, RSO tracking mission can require high slew rates and may provide a torque profile to be met using the cluster. A 3D model of the SGCMG that was simulated has been printed, which confirms the overall size of the actuator; Hardware testing is expected to ensue, starting from basic single actuator testing to confirm the expected properties of a single gimbal, to combining four of the SGCMG into a pyramid cluster to test the torque output of the working cluster.

References

1. Kulu, E., "In-Space Economy in 2021 - Statistical Overview and Classification of Commercial Entities," Proceedings of the 72nd International Astronautical Congress, Dubai, United Arab Emirates, 2021.

2. Sandau, R., "Status and trends of small satellite missions for Earth observation," Acta Astronautica, vol. 66, No. 1-2, 2010.

3. Wiley L. J. and Werts J. R., Space Mission Analysis and Design, Springer, Torrance, 1995.

4. Mumm E., Davis K., Mahin M., Neal D. and Hayes R., "Miniature Control Moment Gyroscope development," Proceedings of the 2014 IEEE Aerospace Conference, Longmont, Colorado, 2014.

5. Arena L., Piergentili F. and Santoni F., "Design, Manufacturing, and Ground Testing of a Control-Moment Gyro for Agile Microsatellites," Journal of Aerospace Engineering, vol. 30, No. 5, 2017.

6. Lappas V., Steyn W. and Underwood C., "Design and testing of a control moment gyroscope cluster for small satellites," Journal of Spacecraft and Rockets, vol. 42, No. 4, 2005.

7. Muñoz J. D., Nagabhushan V., Asundi S. and Fitz-Coy N. G., "High fidelity simulation of SwampSat attitude determination and control system," Advances in Astronautical Sciences, vol. 140, 2011.

8. Wie B., Space Vehicle Dynamics and Control, American Institude of Aeronautics and Astronautics, Reston, 1998.

9. Votel R. and Sinclair D., "Comparison of control moment gyros and reaction wheels for small Earth-orbiting satellites," Proceedings of the 26th Annual AIAA/USU Conference on Small Satellites, Logan, Utah, 2012.

10. Benari G., Joseph T., Podmore H. and Lee R., "Assessing Reaction Wheel Sizing for CubeSat Attitude Control," Toronto, 2018.

11. Wie B., "Singularity Analysis and Visualization for Single-Gimbal Control Moment Gyro Systems," Journal of Guidance, Control, and Dynamics, vol. 27, No. 2, 2004.

12. Vadali S. R., Oh H. S. and Walker S. R., "Preferred gimbal angles for single gimbal control moment gyros," Journal of Guidance, Control, and Dynamics, vol. 13, No. 6, 1990.

13. Kurokawa H., "Survey of theory and steering laws of single-gimbal control moment gyros," Journal of Guidance, Control, and Dynamics, vol. 30, No. 5, 2007.

14. Wie B., Bailey D. and Heiberg C., "Singularity Robust Steering Logic for Redundant Single-Gimbal Control Moment Gyros," Journal of Guidance, Control, and Dynamics, vol. 24, No. 5, pp. 865-872, 2001.